ACS APPLIED MATERIALS & INTERFACES

www.acsami.org

Research Article

Direct Patterning of Optoelectronic Nanostructures Using Encapsulated Layered Transition Metal Dichalcogenides

Teodor K. Stanev,[▽] Pufan Liu,[▽] Hongfei Zeng, Erik J. Lenferink, Akshay A. Murthy, Nathaniel Speiser, Kenji Watanabe, Takashi Taniguchi, Vinayak P. Dravid, and Nathaniel P. Stern*

Cite This: *ACS Appl. Mater. Interfaces* 2022, 14, 23775−23784

Read Online

ACCESS | Metrics & More | Article Recommendations | Supporting Information

ABSTRACT: Direct top-down nanopatterning of semiconductors is a powerful tool for engineering properties of optoelectronic devices. Translating this approach to two-dimensional semiconductors such as monolayer transition metal dichalcogenides (TMDs) is challenging because of both the small scales required for confinement and the degradation of electronic and optical properties caused by high-energy and high-dose electron radiation used for high-resolution top-down direct electron beam patterning. We show that encapsulating a TMD monolayer with hexagonal boron nitride preserves the narrow exciton linewidths and emission intensity typical in such heterostructures after electron beam lithography, allowing direct patterning of functional optical monolayer nanostructures on scales of a few tens of nanometers. We leverage this fabrication method to study size-dependent effects on nanodot arrays of MoS_2 and $MoSe_2$ as well as laterally confined electrical transport devices, demonstrating the potential of top-down lithography for nanoscale TMD optoelectronics.

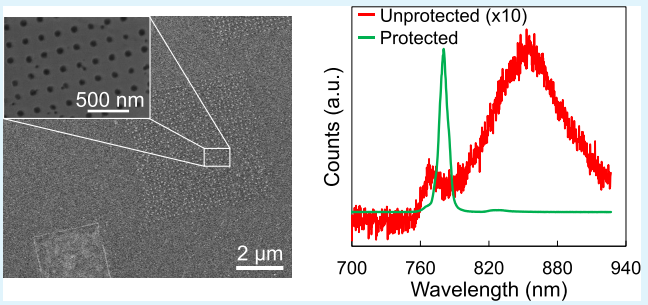

KEYWORDS: *nanopattern, quantum, patterning, defects, monolayer, dichalcogenides*

INTRODUCTION

Engineering of semiconductors in nanoscale structures is a powerful tool for optoelectronic applications. Extending this general approach, nanoscale engineering is now possible using two-dimensional (2D) van der Waals materials by stacking layers in their third, out-of-plane dimension.[1−8] These layered van der Waals heterostructures combining transition metal dichalcogenides (TMDs) and other layered materials facilitate a host of interesting features, such as enhanced optical and electronic properties,[1,2,9−12] new interfacial states,[13−18] improved Ohmic contacts,[19,20] and interlayer band-to-band optical and electronic transitions.[5] Although layered heterostructure engineering with 2D semiconductors like TMDs allows highly tunable optoelectronic properties of the composite structure,[4−6,10,13,16,17,20−22] traditional methods of creating 2D semiconductor nanostructures from layered materials using top-down lateral patterning are not as straightforward. The reduced electronic screening in 2D layers leads to small exciton Bohr radii in TMDs near 1 nm,[23] requiring the creation of smaller nanostructures for significant optoelectronic tuning and emergent phenomena compared to traditional semiconductors that are often too stringent to be achieved using current top-down patterning techniques.

A variety of methods have been identified for realizing TMD nanostructures, including chemically synthesized dots,[24−26] sonicated and centrifuged flakes,[27−30] helium ion-beam patterning,[31,32] direct femtosecond laser writing,[33] laser ablation,[34] electron beam (e-beam) lithography,[35] and gate-defined quantum dots.[36] Some of these approaches, such as sonication and dot synthesis, can achieve very small TMD nanostructures with measurable confinement energies, but they typically lack controllable size, placement, and distribution. Top-down methods based on electron-beam lithography are deterministic and reproducible but face significant impediments for successful application to TMD-based nanostructures due to beam damage. Positive resist (p-resist) electron-beam writing techniques, in which the unexposed resist acts as an etch mask on top of the unetched material, are common for field-effect transistor (FET) lithography and can be used to pattern layered materials down to many tens of nanometers in size.[35] The indirect nature of this patterning technique, however, limits the ultimate nanostructure size to approximately 50 nm,[37] much larger than the Bohr radii of TMDs. Conversely, negative resist (n-resist) techniques use direct writing and can produce patterns down to only several nanometers[38] but require orders of magnitude larger e-beam dosages (~2000 to 1,000,000 $\mu C/cm^2$ for n-resist, compared

Received: February 27, 2022
Accepted: April 28, 2022
Published: May 11, 2022

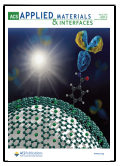

https://doi.org/10.1021/acsami.2c03652
ACS Appl. Mater. Interfaces 2022, 14, 23775−23784

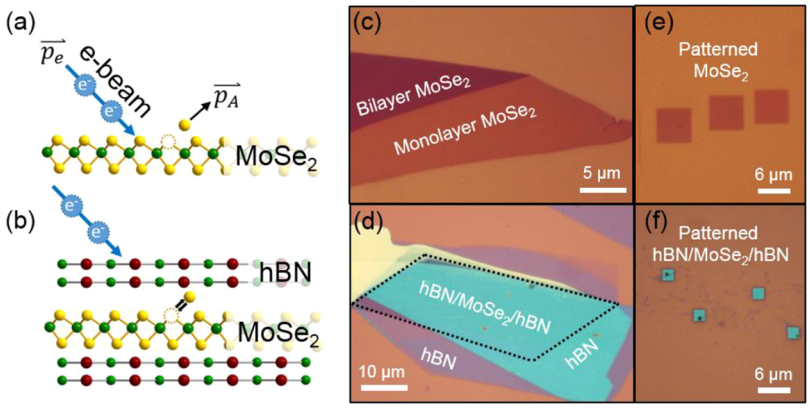

Figure 1. (a) Cartoon of bare $MoSe_2$ being damaged by direct e-beam exposure. Atoms are displaced and the lattice distorted. (b) Encapsulating hBN could protect the TMD layer from direct exposure, preventing the displacement of atoms and distortion of the lattice. (c) Exfoliated $MoSe_2$ monolayer and adjacent bilayer. (d) hBN encapsulated $MoSe_2$ layer achieved by viscoelastic stamping. Black lines outline the $MoSe_2$ under the hBN (teal). A bottom hBN layer (purple) can also be seen. (e) Directly patterned $MoSe_2$ squares from the layer seen in (c). (f) Directly patterned $MoSe_2$ heterostructure squares from the structure seen in (d).

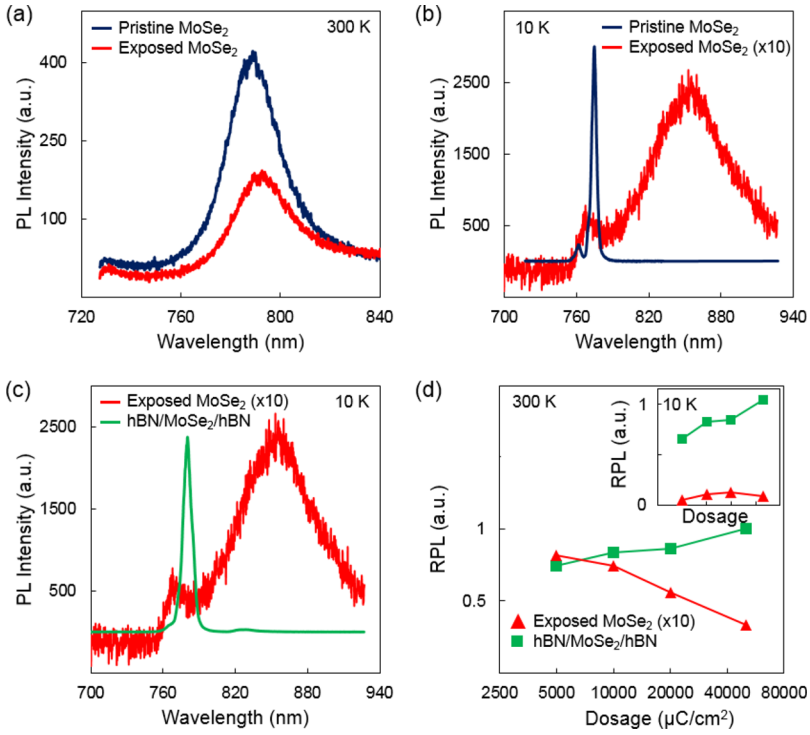

Figure 2. Comparison of PL from e-beam exposed, unencapsulated $MoSe_2$ (exposed) and pristine $MoSe_2$ layer (pristine) at (a) T = 300 K and (b) T = 10 K. At 300 K, e-beam exposure causes a 50% drop in PL intensity and a small shift to lower energy. At 10 K, exposure quenches exciton PL by two orders of magnitude and induces a prominent broad defect emission. (c) Comparison of PL from exposed bare $MoSe_2$ and exposed encapsulated hBN/$MoSe_2$/hBN. The encapsulated layer preserves strong, narrow emission without prominent defect emission. Additional comparison examples can be seen in the SI in Section S1, Figure S3. (d) Relative PL (RPL), defined as the ratio of the integrated intensity of PL from exposed layers to nearby unexposed layers, for exposed bare $MoSe_2$ and hBN/$MoSe_2$/hBN showing the impact of e-beam dosage for direct writing. Inset is 10 K, outset is 300 K; dosage axes are the same. The increasing intensity with dosage for hBN/$MoSe_2$/hBN is attributed to increasing trion emission likely due to charging induced by the intense beam exposure.[40,42]

with ~300 to 1000 $\mu C/cm^2$ for p-resist). This has been found to cause destructive damage to the target-layered crystal that degrades optoelectronic characteristics.[39−42] Adapting n-resist patterning for the top-down lithography of TMD nanostructures at the relevant size scales requires overcoming the intrinsic layer damage caused by the high e-beam dosage.

One promising means to overcome this practical challenge is to combine traditional top-down lithography with novel vertical engineering afforded by 2D materials. Interfacing TMD flakes with a layer of hexagonal boron nitride (hBN), a wide band gap van der Waals material, can protect underlying TMD layers from atmospheric degradation[43] or substrate defects.[44] With the encapsulation of a TMD between two thin layers of hBN, hBN/TMD/hBN heterostructures can exhibit exciton emission linewidths approaching fundamental limits[1,10] and device mobilities in the hundreds to thousands of cm^2/Vs.[3] Here, we show that the hBN/TMD/hBN heterostructure also allows for the direct e-beam patterning of TMDs under n-

https://doi.org/10.1021/acsami.2c03652
ACS Appl. Mater. Interfaces 2022, 14, 23775−23784

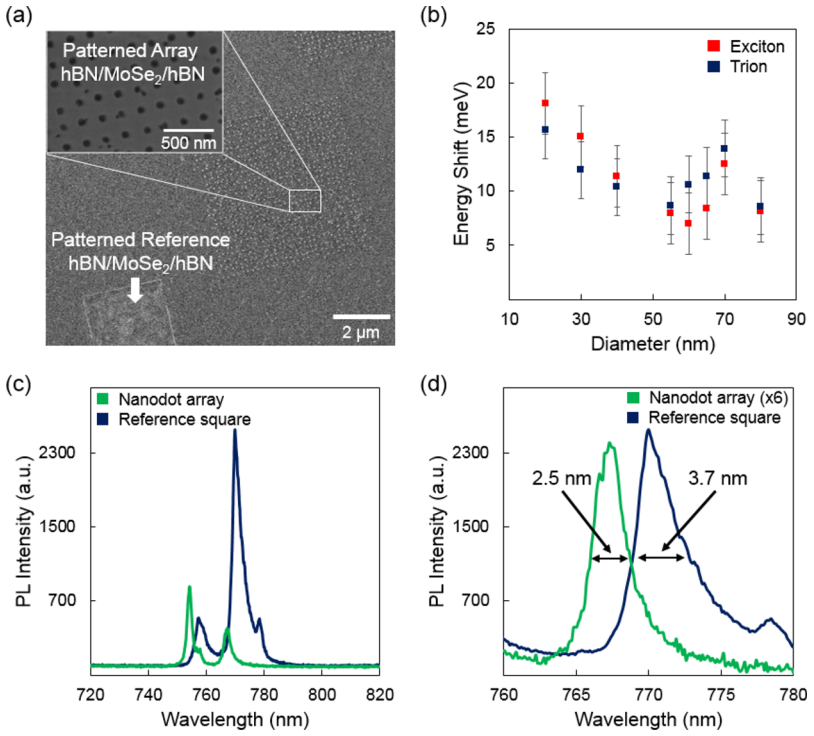

Figure 3. (a) Patterned array of $MoSe_2$ nanodots with diameter of 40 nanometers. A reference square of unpatterned hBN/$MoSe_2$/hBN is visible in the bottom left. (b) Average exciton and trion energy shift for different nanodot diameters. The shift is measured relative to an exposed reference square to rule out contributions from e-beam exposure not related to size. At small dot diameters, a small size-dependent energy shift can be seen. At large dot diameters, the energy shift does not vanish, suggesting that size-independent energy shift is also present. The error bars represent the averaged standard deviation of five samples at 40 nm dot size. (c) Plot of PL of patterned dots of $MoSe_2$ with a diameter of 40 nm and patterned referenced square of $MoSe_2$. We see a distinct shift in exciton population from the trion state to the neutral state and an overall quenching of PL due to the loss of total material after patterning. (d) Zoom in on the trion PL of the patterned array of dots emitter (40 nm diameter, array in SEM image Figure 3a) to the reference square, showing an energy shift of ~6 meV and a linewidth reduction.

resist to achieve repeatable nanofabrication down to ten nanometer feature scales without significantly damaging the underlying layer. The optical and electrical qualities are preserved even with high-dosage patterning, allowing for sharp linewidths and high mobilities in TMD nanostructures. Simple representations of the e-beam induced damage and a hypothetical hBN-afforded protection mechanism are shown in Figure 1a,b, respectively, illustrating how encapsulation may offer protection from the formation of chalcogenide vacancies.

We leverage this direct writing capability for the creation of nanometer scale nanodots, revealing weak size-dependent energy shifts, and for top-down patterning of narrow electronic device nanochannels of a few tens of nanometers that demonstrate quantized conduction.

RESULTS AND DISCUSSION

To study layer damage and nanopatterning, monolayer flakes of $MoSe_2$ and few-layer flakes of high-quality hBN were prepared by micromechanical exfoliation on 285 nm SiO_2 on Si substrates and identified by optical contrast, as shown in Figure 1c. Heterostructures of monolayer $MoSe_2$ flakes encapsulated by hBN were then assembled by viscoelastic stamping[45] (Figure 1d). Both the heterostructures and unencapsulated monolayers of $MoSe_2$ were annealed in an Ar/H_2 environment to improve surface quality and adhesion, remove transfer, and exfoliation residues such as tape adhesive. Atomic force microscopy was used to confirm a uniform, flat surface free from any wrinkles and folds that can be introduced in the transfer process. Subsequently, the heterostructures were characterized using photoluminescence (PL) spectroscopy to confirm narrow emission linewidths typical of hBN-encapsulated $MoSe_2$.[1,10] Both the encapsulated and unencapsulated $MoSe_2$ monolayers were patterned with standard electron beam lithography using n-resist into squares with an edge size of 3 μm, as seen in Figure 1e,f. The writing was performed using a 100 keV e-beam lithography system with 10 nm hydrogen silsesquioxane (HSQ) as the n-resist with dosages varying from 5000 to 50,000 $\mu C/cm^2$[38] to test layer damage thresholds.

PL measurements were performed at temperatures of 10 and 300 K for patterned encapsulated (hBN/$MoSe_2$/hBN), patterned unencapsulated, and pristine unprocessed $MoSe_2$ (Figure 2a–d). Room temperature PL from unencapsulated monolayers in Figure 2a shows a reduction in intensity compared to that in pristine unprocessed layers, likely due to the extensive layer damage from the direct e-beam writing. At a low temperature, where emission from the exciton and trion (an exciton with an extra bound electron) correspond to distinct peaks as shown in Figure 2b, this damage is especially evident as the PL intensity in the unencapsulated layer is quenched by two orders of magnitude and a broad emission emerges across the 800–900 nm spectrum. This broad defect emission is orders of magnitude brighter than that observed for unexposed $MoSe_2$, and it is typically attributed to significant damage to the $MoSe_2$ crystal structure from the high dose direct e-beam exposure.[39,41,42] In contrast, the encapsulated structure of hBN/$MoSe_2$/hBN in Figure 2c shows no

https://doi.org/10.1021/acsami.2c03652
ACS Appl. Mater. Interfaces 2022, 14, 23775−23784

significant defect emission and a strong, narrow exciton PL peak even after direct e-beam writing.

Damage from the direct beam exposure was characterized by varying the dosage on multiple patterned squares, as shown in Figure 2d. Unsurprisingly, increasing dosage rapidly degrades the unencapsulated layer, with 20,000 $\mu C/cm^2$ inducing a roughly 50% quenching of the PL in the unencapsulated layer at room temperature and orders of magnitude of quenching at low temperature (Figure 2d (inset)). A strong defect emission (relative to neutral and trion emission) also emerges in the exposed bare layer, signifying significant structural damage to the crystal. Further visualizations of e-beam induced damage using 2D PL mapping before and after direct e-beam exposure are in the Supporting Information in Figures S1 and S2. An equivalent exposure to the encapsulated $MoSe_2$ layer only marginally diminishes the PL intensity, as seen in Figure 2d. Evidently, combining hBN encapsulation with high-dose direct e-beam writing allows high-resolution top-down patterning of monolayer TMD nanostructures without significantly compromising optical quality.

We have shown that hBN encapsulation enables direct e-beam lithography of TMDs without significantly damaging the crystal and quenching optical emission. A possible explanation for this effect is that encapsulation could increase the threshold energy for chalcogenide atoms to escape the TMD monolayer (shown previously in Figure 1a,b). Interactions between TMD layers and high energy electrons can result in extensive radiolysis, lattice deformation, and amorphization.[39,41,42] In unencapsulated material, a chalcogenide atom only needs to acquire enough energy to break the TMD covalent bond to escape, which can be readily provided by a 100 keV e-beam. However, with hBN encapsulation, displaced atoms must also diffuse past the hBN layer or break the hBN covalent bonds to escape. The higher threshold energy prevents this from occurring,[32] evidenced here by the preserved excitonic features in PL and the absence of strong defect emission at low temperature. It is, however, possible that the hBN top layer experiences damage from the e-beam dosage, but this top layer would serve as a sacrificial layer, and damage to the hBN structure would not have been observable in the present measurements and is not studied in more detail here. The small reduction in PL intensity with hBN encapsulation (Figure 2d) suggests that this protection is not perfect or that the electron bombardment can still cause charge doping. Although mechanistic testing of this explanation is beyond the scope of experiments performed here, the experimental results do indicate clearly that hBN-encapsulated TMDs can help prevent e-beam damage and allow direct writing of TMD nanostructures with good optical quality.

Utilizing this high-resolution top-down lithography enabled by hBN encapsulation, size-dependent PL from patterned TMD nanostructures of variable radii was studied. Square arrays (side length of 6 μm) of hBN/$MoSe_2$/hBN nanodots with diameters ranging from 10 to 80 nm and nanodot spacing of 200 nm were fabricated with the procedures described previously along with squares of side length of 3 μm for reference (Figure 3a). The reference squares were exposed to the same e-beam dosage as the nanodots, allowing the isolation of beam-induced effects from size and edge effects. Sub-10 nm nanodots with diameters down to 5 nm were also fabricated, but in these small nanodots, the n-resist typically loses adhesion to the layer surface, resulting in nanodot aggregation or complete pattern loss (see Figure S4 in the Supporting Information for the visualization of this behavior). SEM images (Supporting Information Figure S5) suggest that after etching, small diameter nanodots were still successfully created, but their position and separation are no longer controllable and repeatable. Based on the results in Figures 2 and 3, optical damage is no longer the limiting constraint in the size of patterning. The adhesion problem shown in Supporting Information Figure S5 remains a challenge to overcome that would allow the smallest patterns possible with negative resist. Further systematic study of resist and process steps could improve the surface adhesion and allow controlled patterning of sub-10 nm nanostructures without inducing layer damage, but this process development is beyond the scope of the current work.

Following fabrication, PL was measured from the arrays in vacuum at temperatures of both 10 and 300 K, sampling an ensemble of approximately 25 nanodots per 1 μm beam spot because the arrays have a 200 nm spacing. While strong exciton PL peaks at room temperature in the nanodot arrays provided a good indication of nondestructive direct writing and etching, the linewidths were too broad to extract small size-dependent energy shifts possibly caused by confinement or edge effects.[35] In contrast, at low temperature, linewidths of $MoSe_2$ can approach single-digit meV scales,[1,10,46] distinctly separating out the exciton and trion species and enhancing sensitivity to small energy shifts. PL results at 10 K can be seen in Figure 3a−d.

For nanodots with diameters from 80 nm down to 20 nm, the emission energies of both the exciton and trion show a weak size-dependent shift toward higher energy (Figure 3b,c) and reduced linewidths as compared to the nearby reference squares to rule out potential e-beam contributions (Figure 3d). The shift can be parameterized by a size-independent shift present in even the largest nanodots (but not the reference squares) and an additional weak shift to higher energies when decreasing the nanodot size. Although these experiments do not conclusively identify the origin of the size-dependent shift, these nanodots would be in a weak confinement regime because they are larger than the exciton Bohr radius. The larger size-independent energy shift of average ∼10 meV seen on all patterns is not exciton confinement related and is likely introduced by the fabrication process. Because shift to higher emission energies was not observed in the reference square, which was written in an identical fashion to the nanodots, the energy shifts in PL were not introduced by e-beam exposure itself. The origin of the smaller size-dependent energy blue shift is not conclusively identified by these experiments.

One possible cause for the large size-independent shift seen for all nanodot diameters is an edge effect. Unlike the reference square, the reduced size of the nanodots significantly modifies the edge-to-surface area ratio, making edge effects such as roughness or edge doping much more significant. While localized edge states are unlikely to have much influence on larger dots because of their limited interaction depth,[47] contributions from edge doping created through the etching process can extend out to ∼10 nm[48] and may be non-negligible in nanodot PL. It should be noted that as the diameter of the dots increases from 20 to 80 nm, the magnitude of the background shift fades as the cross-sectional area of the dot increases, suggesting that this is an edge effect. As the dot diameter approaches 60−80 nm, we begin to see a mixture of unshifted exciton emission and shifted exciton emission

https://doi.org/10.1021/acsami.2c03652
ACS Appl. Mater. Interfaces 2022, 14, 23775−23784

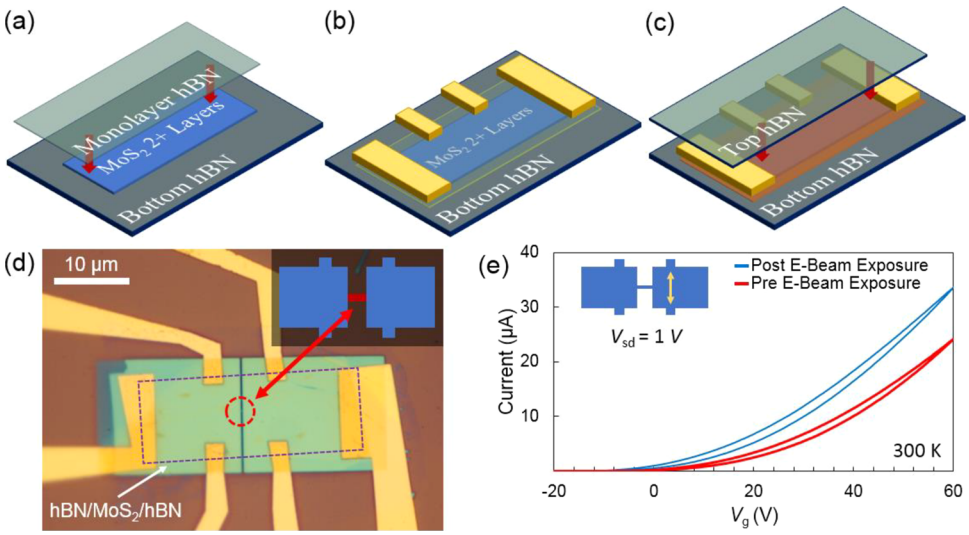

Figure 4. (a–c) Preparation of the MoS_2 layer for the electrical device. (a) Few-layer MoS_2 is transferred onto an hBN bottom layer, followed by a multilayer of hBN on the top to serve as a tunneling layer. (b) Contacts are deposited on the top of the monolayer of hBN. (c) A final multilayer of hBN is transferred on the top of the completed structure for protection. (d) An image of a completed electrical device, represented schematically in the inset. The patterned conduction channel is highlighted red. A purple dotted line outlines the monolayer under the hBN. (e) Current vs gate voltage (V_G) performance before (red) and after (blue) e-beam exposure for a hBN/MoS_2/hBN heterostructure for a two-terminal nonchannel test as the inset shows. To test the impact of exposure on bulk transport, this device is patterned with the n-resist process with a dosage of 50,000 $\mu C/cm^2$ over the entire heterostructure area in contrast to the nanochannel patterning described in the Methods. Exposure changes estimated mobility from 45 to 48 cm^2/Vs, extracted from the slope. The higher current response suggests an increased n-type doping of the material after exposure, but there is no reduction in electrical performance that would indicate layer damage from exposure.

because of edge-state contributions (see Figure S6 in the Supporting Information).

We attribute the linewidth reduction after e-beam patterning to a reduced crystal inhomogeneity.[49−53] It is well-known that the optical properties of TMDs are very sensitive to strain,[54] and as such, reduced strain inhomogeneity can result in reduced linewidths compared to larger hBN encapsulated $MoSe_2$. In the reference square case, the layer would be a large continuous sheet susceptible to sources of inhomogeneity such as bubble-induced strain,[55] on which direct writing would have no impact. It is not until the layer is broken down into discrete few-nanometer discs that inhomogeneity is reduced as nonlocal effects are suppressed.

Transition electron microscopy (TEM) study of exposed layers and their edges could further elucidate the lattice damage of e-beam exposure and its reduction with hBN protection. Although promising, implementing these TEM measurements for nanodots and their edges would require the development of new approaches for TEM sample preparation extending beyond the methods currently available for monolayers,[56] which is beyond the scope of what is studied here. Rather, we use the optical properties as a probe for inferring the impact of e-beam exposure that cannot be imaged directly in nanodots.

Having established that hBN encapsulation can preserve optical properties of patterned TMD monolayer nanostructures, the utility of this approach for nanoelectronic devices was tested. TMD nanochannels have been shown previously to exhibit quantized conduction using optical doping and gate-defined transport[21,57,58] but not in patterned nanostructures. Given that hBN encapsulation preserves the optical properties of TMDs, we further test its potential to realize nanoscale electronic devices and quantum conductance channels. Here, we use the same techniques via hBN encapsulation, but switch to MoS_2 instead of $MoSe_2$ because of the depth of the literature for MoS_2 FETs reporting high mobilities,[2,3,59] to demonstrate the creation of quantized conductive channels.

High-mobility MoS_2 achieved with hBN encapsulation is a good candidate for quantum conduction and direct e-beam writing with mobilities typically exceeding 50−100 cm^2/Vs[2,3,59] for monolayers. Even higher mobilities are possible in multilayers, with record reported Hall mobility of 37,000 cm^2/Vs in six-layer MoS_2.[59] Samples were made of hBN/2−4 L MoS_2/1 L hBN heterostructures patterned with e-beam lithography. Gold contacts were deposited using standard procedures.[2] Few-layer MoS_2 was used for the nanoelectrical devices because they achieve higher mobility compared to a single-layer device.[3] Multilayer MoS_2 is not thick enough to be self-protected from e-beam damage and still requires hBN protection to preserve high mobility in n-resist lithography much like monolayers.[60] The single layer of hBN on top serves as a tunnel barrier for Ohmic electrical contacts[20] while also protecting the TMD layer from external adsorbates and perturbations, leading to enhanced mobility.[2,3] A second flake of few-layer hBN was transferred on top of the fully fabricated contacts and unpatterned MoS_2 to ensure sufficient protection for the nanochannel region. The conducting channel device was then patterned with direct n-resist lithography using the same procedures described for $MoSe_2$. The stacking and contact process and final device can be seen in Figure 4a–d.

An hBN-encapsulated MoS_2 heterostructure was electrically tested before and after direct e-beam exposure, as seen in Figure 4e. Two-terminal conductivity showed no appreciable electrical damage caused by direct exposure, as the overall field-effect mobilities at room temperature (45 cm^2/Vs before to 48 cm^2/Vs after) and low temperature (43 to 50 cm^2/Vs) were largely unaffected. The turn-on threshold gate voltage of the encapsulated device was larger after writing, which is not unexpected following extensive electron bombardment and charging of the material.

https://doi.org/10.1021/acsami.2c03652
ACS Appl. Mater. Interfaces 2022, 14, 23775−23784

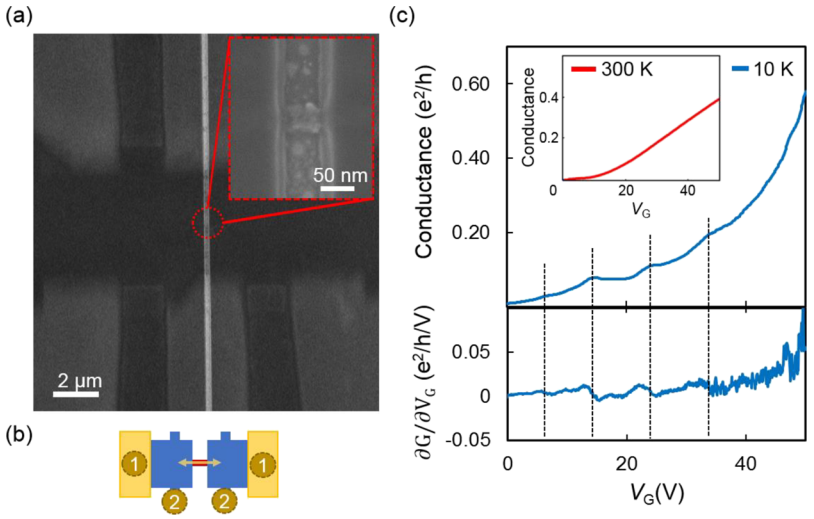

Figure 5. (a) SEM image of the patterned device with a narrow channel at the center. (Inset) Zoom in on channel. (b) Simple cartoon representation of device measurement from (a) in a four-terminal arrangement. Contacts 1 are used as source and drain for current, and Contacts 2 are used for sensing in a four-terminal experiment. (c) Measured conductance as a function of gate voltage across a 50 nm wide channel etched into an hBN/MoS_2/hBN heterostructure, as seen in the inset of (a). Inset is 300 K, and outset is 10 K. Step-like behavior can be observed at 10 K, but no such features can be seen at 300 K. (Bottom) Derivative of the conductance with respect to the applied gate voltage. Peaks and dips correspond to the step-like transitions. Black dashed lines serve as a guide to the eye.

Conduction channels of 50 nm width and 100 nm length were fabricated at the center of a six-terminal Hall bar electrical contact geometry similar to the device seen in Figure 4d. An SEM image of a channel can be seen in Figure 5a. Four-terminal conductance measurements were performed across the channel using the source and drain leads and their corresponding adjacent sense-leads on either side of the channel. At cryogenic temperatures (10 K), the channel shows discrete steps in conductance at regular gate voltage intervals ($V_G \sim$ 6.7, 14.5, 24.9, and 34.5 V), a hallmark of quantized conduction.[21,36,57,61−63] This is further confirmed by noting that the energy spacing of the observed quantized levels are higher than thermal energy at 10 K, and the Fermi wavelength of electrons are comparable to the channel width (see Supporting Information Section S6 for details). These conductance plateaus shown in Figure 5b are however not integer values; this is likely due to the sample geometry (see SI Section S7) and is consistent with previous measurements of quantum channels in MoS_2.[57,58] At room temperature, conductance showed the behavior of a classical MoS_2 FET, as seen in Figure 5c (inset), much like the behavior seen in Figure 4e for bulk sheets of MoS_2, which is in accordance with expectations.

Previous observations of quantized conduction utilized indirect control of the layer's size via optically doped restrictions or backgate-defined channels.[21,57,58] Here, we have directly and precisely patterned the TMD conducting channel down to a quantum-confined limit using traditional top-down lithography, which is a key ingredient for the deterministic patterning of layered nanostructures with quantum transport effects. Thicker heterostructures result in more screening of gating and optical effects, posing limits on quantum nanodevices prepared through such methods.[64,65] Our techniques allow direct patterning useful for quantum conduction in more complex and intriguing engineered layered heterostructures.[4,6,22]

CONCLUSIONS

In summary, we have shown the ability of hBN encapsulation to protect monolayer TMDs from damage from high-dose e-beam irradiation, thereby allowing for the controlled and repeatable patterning of monolayers at the 10 nm scale with good optoelectronic properties. Optical and electrical features of layers patterned in nanostructures using this method were explored in both optical emission from encapsulated $MoSe_2$ nanodots and quantized transport behavior in narrow MoS_2 channels. These examples demonstrate that our nondestructive patterning technique can enable direct, deterministic patterning of laterally confined TMD nanoelectronics, thereby expanding the toolkit available for quantum electronic devices from layered heterostructures.

METHODS

van der Waals heterostructures were assembled by first exfoliating individual components with tape-assisted micromechanical exfoliation[66,67] on 285 nm SiO_2 on silicon substrates. Pieces were then lifted from SiO_2 using a polycarbonate (PC) stamp on polydimethylsiloxane (PDMS) supported by a glass slide and placed upon a prepatterned chip with gold leads that served as both contacts for electrical devices in later steps and identification markers for optical measurements. Few-layer flakes of hBN to form the heterostructure bottom layers were lifted and placed onto the target SiO_2, cleaned of PC with chloroform and isopropyl alcohol (IPA) baths, and then annealed at 400 °C for 2 h to improve surface adhesion and remove residue. Subsequent layers were moved and cleaned in a similar fashion to create hBN/TMD/hBN heterostructures. For the electrical devices, after the hBN/TMD/monolayer hBN heterostructure was prepared, the sample was spun with a methyl methacrylate and poly(methyl methacrylate) (MMA/PMMA) mask, and contacts were written with e-beam lithography over the monolayer hBN over the MoS_2 layer to create tunneling contacts. Gold was deposited by thermal evaporation followed by lift off in an acetone bath at 60 °C for 30 min. A final layer of hBN was then placed on the top of the completed device to protect from direct e-beam writing. The full device was cleaned a final time in chloroform and IPA wash and then annealed.

Patterning was performed with a 100 keV e-beam lithography system (JBX-9300FS). For optical devices, hydrogen silsesquioxane

https://doi.org/10.1021/acsami.2c03652
ACS Appl. Mater. Interfaces 2022, 14, 23775−23784

(HSQ) was used as the negative resist for the patterning. HSQ (10 nm) was first spin coated onto the sample, and then, nanodot patterns were written with e-beam. Depending on the pattern feature size, the dosage applied varied from 10,000 to 1000,000 $\mu C/cm^2$ as smaller features require higher dosage. The exposed sample was then developed in CD-26 at 50 ° C for 2 min and etched with a reactive ion etcher (Oxford Plasma Lab 100). The geometry of the channel (in Figures 5 or S5) is a horizontal narrow channel in the center of a vertical narrow gap. Because of the proximity effect, this structure will be difficult to write in one step with either n-resist or p-resist. Therefore, this structure is written in two steps. The first step uses n-resist (20 nm HSQ) with methods and dosages analogous to optical devices previously discussed to write the horizontal narrow channel, and the second step uses p-resist (50 nm GL-2000) to write the vertical narrow gap. The GL-2000 resist after spin-coating was first baked at 180 °C for 3 min and then written with e-beam with the dosage varying from 500 to 5000 $\mu C/cm^2$. The sample was then developed in n-amyl-acetate at 0 °C for 1 min and etched with a reactive ion etcher (Oxford Plasma Lab 100), thus defining the geometry of the device.

Optical and electrical measurements were performed in a closed-cycle 4 K optical cryostat (Advanced Research Systems DE204PF). Photoluminescence spectra were collected on a spectrometer (Andor Shamrock SR-750) with a CCD camera (iDUS DU420-A) using illumination from a 532 nm diode pumped solid-state laser (Lighthouse Photonics Sprout-G-15 W). Electrical measurements were performed using a source-measure unit (Keithley 2614B) for electrical biasing and gating and a nanovoltmeter (Keithley 2182A) for voltage sensing in a four-terminal configuration.

■ ASSOCIATED CONTENT

Supporting Information

The Supporting Information is available free of charge at https://pubs.acs.org/doi/10.1021/acsami.2c03652.

PL mapping of direct e-beam exposure damage, AFM characterization of the transfer process, SEM imaging of poor adhesion in small nanodots, multiple exciton emission signatures in large nanodots, spatial variation in exciton and trion spectral components, discussion of characteristic energy and length scales, and discussion of subinteger conduction plateaus (PDF)

■ AUTHOR INFORMATION

Corresponding Author

Nathaniel P. Stern − *Department of Physics and Astronomy, Northwestern University, Evanston, Illinois 60208, United States;* orcid.org/0000-0002-8903-3516; Email: n-stern@northwestern.edu

Authors

Teodor K. Stanev − *Department of Physics and Astronomy, Northwestern University, Evanston, Illinois 60208, United States*

Pufan Liu − *Department of Materials Science and Engineering, Northwestern University, Evanston, Illinois 60208, United States*

Hongfei Zeng − *Department of Physics and Astronomy, Northwestern University, Evanston, Illinois 60208, United States*

Erik J. Lenferink − *Department of Physics and Astronomy, Northwestern University, Evanston, Illinois 60208, United States*

Akshay A. Murthy − *Department of Materials Science and Engineering, Northwestern University, Evanston, Illinois 60208, United States;* orcid.org/0000-0001-7677-6866

Nathaniel Speiser − *Department of Physics and Astronomy, Northwestern University, Evanston, Illinois 60208, United States*

Kenji Watanabe − *Research Center for Functional Materials and International Center for Materials Nanoarchitectonics, National Institute for Materials Science, Tsukuba 305-0044, Japan;* orcid.org/0000-0003-3701-8119

Takashi Taniguchi − *Research Center for Functional Materials and International Center for Materials Nanoarchitectonics, National Institute for Materials Science, Tsukuba 305-0044, Japan;* orcid.org/0000-0002-1467-3105

Vinayak P. Dravid − *Department of Materials Science and Engineering and International Institute for Nanotechnology (IIN), Northwestern University, Evanston, Illinois 60208, United States; Northwestern University Atomic and Nanoscale Characterization Experimental (NUANCE) Center, Northwestern University, Evanston, Illinois 60208, United States;* orcid.org/0000-0002-6007-3063

Complete contact information is available at: https://pubs.acs.org/10.1021/acsami.2c03652

Author Contributions

[▽]T.K.S. and P.L. contributed equally to this work.

Author Contributions

The manuscript was written through contributions of all authors. All authors have given approval to the final version of the manuscript.

Notes

The authors declare no competing financial interest.

■ ACKNOWLEDGMENTS

This work was primarily supported by the Office of Naval Research under Grant No. N00014-16-1-3055. Sample fabrication and characterization were supported by the National Science Foundation's MRSEC program (DMR-1720139) at the Materials Research Center of Northwestern University and by Argonne National Laboratory. This work made use of the EPIC, Keck-II, SPID, and NUFAB facilities of Northwestern University's NUANCE Center, which has received support from the SHyNE Resource (NSF ECCS-2025633), the IIN, and Northwestern's MRSEC program (NSF DMR-1720139). Use of the Center for Nanoscale Materials, an Office of Science user facility, was supported by the U.S. Department of Energy, Office of Science, Office of Basic Energy Sciences, under Contract No. DE-AC02-06CH11357. K.W. and T.T. acknowledge support from the Elemental Strategy Initiative conducted by the MEXT, Japan (Grant Number JPMXP0112101001) and JSPS KAKENHI (Grant Nos. 19H05790, 20H00354 and 21H05233). A.A.M. and V.P.D. acknowledge support from the National Science Foundation under Grant No. DMR-1929356. A.A.M. also gratefully acknowledges support from the Ryan Fellowship and the IIN at Northwestern University.

■ REFERENCES

(1) Ajayi, O. A.; Ardelean, J. V.; Shepard, G. D.; Wang, J.; Antony, A.; Taniguchi, T.; Watanabe, K.; Heinz, T. F.; Strauf, S.; Zhu, X. Y.; Hone, J. C. Approaching the Intrinsic Photoluminescence Linewidth in Transition Metal Dichalcogenide Monolayers. *2D Mater.* **2017**, *4*, No. 031011.

(2) Lee, G.-H.; Cui, X.; Kim, Y. D.; Arefe, G.; Zhang, X.; Lee, C.-H.; Ye, F.; Watanabe, K.; Taniguchi, T.; Kim, P.; Hone, J. Highly Stable, Dual-Gated MoS_2 Transistors Encapsulated by Hexagonal Boron Nitride With Gate-Controllable Contact, Resistance, and Threshold Voltage. *ACS Nano* **2015**, *9*, 7019−7026.
(3) Wang, J.; Yao, Q.; Huang, C.-W.; Zou, X.; Liao, L.; Chen, S.; Fan, Z.; Zhang, K.; Wu, W.; Xiao, X.; Jiang, C.; Wu, W.-W. High Mobility MoS_2 Transistor with Low Schottky Barrier Contact by Using Atomic Thick hBN as a Tunneling Layer. *Adv. Mater.* **2016**, *28*, 8302−8308.
(4) Rivera, P.; Schaibley, J. R.; Jones, A. M.; Ross, J. S.; Wu, S.; Aivazian, G.; Klement, P.; Seyler, K.; Clark, G.; Ghimire, N. J.; Yan, J.; Mandrus, D. G.; Yao, W.; Xu, X. Observation of Long-Lived Interlayer Excitons in Monolayer $MoSe_2$−WSe_2 Heterostructures. *Nat. Commun.* **2015**, *6*, 6242.
(5) Ross, J. S.; Rivera, P.; Schaibley, J.; Lee-Wong, E.; Yu, H.; Taniguchi, T.; Watanabe, K.; Yan, J.; Mandrus, D.; Cobden, D.; Yao, W.; Xu, X. Interlayer Exciton Optoelectronics in a 2D Heterostructure P−N Junction. *Nano Lett.* **2017**, *17*, 638−643.
(6) Tran, K.; Moody, G.; Wu, F.; Lu, X.; Choi, J.; Kim, K.; Rai, A.; Sanchez, D. A.; Quan, J.; Singh, A.; Embley, J.; Zepeda, A.; Campbell, M.; Autry, T.; Taniguchi, T.; Watanabe, K.; Lu, N.; Banerjee, S. K.; Silverman, K. L.; Kim, S.; Tutuc, E.; Yang, L.; MacDonald, A. H.; Li, X. Evidence for Moiré Excitons in Van Der Waals Heterostructures. *Nature* **2019**, *567*, 71−75.
(7) Kretinin, A. V.; Cao, Y.; Tu, J. S.; Yu, G. L.; Jalil, R.; Novoselov, K. S.; Haigh, S. J.; Gholinia, A.; Mishchenko, A.; Lozada, M.; Georgiou, T.; Woods, C. R.; Withers, F.; Blake, P.; Eda, G.; Wirsig, A.; Hucho, C.; Watanabe, K.; Taniguchi, T.; Geim, A. K.; Gorbachev, R. V. Electronic Properties of Graphene Encapsulated with Different Two-Dimensional Atomic Crystals. *Nano Lett.* **2014**, *14*, 3270−3276.
(8) Ferrari, A. C.; Bonaccorso, F.; Fal'ko, V.; Novoselov, K. S.; Roche, S.; Bøggild, P.; Borini, S.; Koppens, F. H. L.; Palermo, V.; Pugno, N.; Garrido, J. A.; Sordan, R.; Bianco, A.; Ballerini, L.; Prato, M.; Lidorikis, E.; Kivioja, J.; Marinelli, C.; Ryhänen, T.; Morpurgo, A.; Coleman, J. N.; Nicolosi, V.; Colombo, L.; Fert, A.; Garcia-Hernandez, M.; Bachtold, A.; Schneider, G. F.; Guinea, F.; Dekker, C.; Barbone, M.; Sun, Z.; Galiotis, C.; Grigorenko, A. N.; Konstantatos, G.; Kis, A.; Katsnelson, M.; Vandersypen, L.; Loiseau, A.; Morandi, V.; Neumaier, D.; Treossi, E.; Pellegrini, V.; Polini, M.; Tredicucci, A.; Williams, G. M.; Hee Hong, B.; Ahn, J.-H.; Min Kim, J.; Zirath, H.; van Wees, B. J.; van der Zant, H.; Occhipinti, L.; Di Matteo, A.; Kinloch, I. A.; Seyller, T.; Quesnel, E.; Feng, X.; Teo, K.; Rupesinghe, N.; Hakonen, P.; Neil, S. R. T.; Tannock, Q.; Löfwander, T.; Kinaret, J. Science and Technology Roadmap for Graphene, Related Two-Dimensional Crystals, and Hybrid Systems. *Nanoscale* **2015**, *7*, 4598−4810.
(9) Han, X.; Lin, J.; Liu, J.; Wang, N.; Pan, D. Effects of Hexagonal Boron Nitride Encapsulation on the Electronic Structure of Few-Layer MoS_2. *J. Phys. Chem. C* **2019**, *123*, 14797−14802.
(10) Cadiz, F.; Courtade, E.; Robert, C.; Wang, G.; Shen, Y.; Cai, H.; Taniguchi, T.; Watanabe, K.; Carrere, H.; Lagarde, D.; Manca, M.; Amand, T.; Renucci, P.; Tongay, S.; Marie, X.; Urbaszek, B. Excitonic Linewidth Approaching the Homogeneous Limit in MoS_2-Based Van Der Waals Heterostructures. *Phys. Rev. X* **2017**, *7*, No. 021026.
(11) Li, Q.; Xu, L.; Luo, K.-W.; Li, X.-F.; Huang, W.-Q.; Wang, L.-L.; Yu, Y.-B. Electricfield Induced Widely Tunable Direct and Indirect Band Gaps in hBN/MoS_2 Van Der Waals Heterostructures. *J. Mater. Chem. C* **2017**, *5*, 4426−4434.
(12) Lee, C.; Rathi, S.; Khan, M. A.; Lim, D.; Kim, Y.; Yun, S. J.; Youn, D.-H.; Watanabe, K.; Taniguchi, T.; Kim, G.-H. Comparison of Trapped Charges and Hysteresis Behavior in hBN Encapsulated Single MoS_2 Flake Based Field Effect Transistors on SiO_2 and hBN Substrates. *Nanotechnology* **2018**, *29*, 335202.
(13) Calman, E. V.; Fogler, M. M.; Butov, L. V.; Hu, S.; Mishchenko, A.; Geim, A. K. Indirect Excitons in Van Der Waals Heterostructures at Room Temperature. *Nat. Commun.* **2018**, *9*, 1895.
(14) Wang, S.; Tian, H.; Ren, C.; Yu, J.; Sun, M. Electronic and Optical Properties of Heterostructures Based on Transition Metal Dichalcogenides and Graphene-Like Zinc Oxide. *Sci. Rep.* **2018**, *8*, 12009.
(15) Li, M.-Y.; Chen, C.-H.; Shi, Y.; Li, L.-J. Heterostructures Based on Two-Dimensional Layered Materials and Their Potential Applications. *Mater. Today* **2016**, *19*, 322−335.
(16) Choi, W.; Akhtar, I.; Rehman, M. A.; Kim, M.; Kang, D.; Jung, J.; Myung, Y.; Kim, J.; Cheong, H.; Seo, Y. Twist-Angle-Dependent Optoelectronics in a Few-Layer Transition-Metal Dichalcogenide Heterostructure. *ACS Appl. Mater. Interfaces* **2019**, *11*, 2470−2478.
(17) Li, C.; Cao, Q.; Wang, F.; Xiao, Y.; Li, Y.; Delaunay, J.-J.; Zhu, H. Engineering Graphene and TMDs Based Van Der Waals Heterostructures for Photovoltaic and Photoelectrochemical Solar Energy Conversion. *Chem. Soc. Rev.* **2018**, *47*, 4981−5037.
(18) Wang, H.; Liu, F.; Fu, W.; Fang, Z.; Zhou, W.; Liu, Z. Two-Dimensional Heterostructures: Fabrication, Characterization, and Application. *Nanoscale* **2014**, *6*, 12250−12272.
(19) Cui, X.; Shih, E.-M.; Jauregui, L. A.; Chae, S. H.; Kim, Y. D.; Li, B.; Seo, D.; Pistunova, K.; Yin, J.; Park, J.-H.; Choi, H.-J.; Lee, Y. H.; Watanabe, K.; Taniguchi, T.; Kim, P.; Dean, C. R.; Hone, J. C. Low-Temperature Ohmic Contact to Monolayer MoS_2 by Van Der Waals Bonded Co/hBN Electrodes. *Nano Lett.* **2017**, *17*, 4781−4786.
(20) Murthy, A. A.; Stanev, T. K.; Cain, J. D.; Hao, S.; LaMountain, T.; Kim, S.; Speiser, N.; Watanabe, K.; Taniguchi, T.; Wolverton, C.; Stern, N. P.; Dravid, V. P. Intrinsic Transport in 2D Heterostructures Mediated Through hBN Tunneling Contacts. *Nano Lett.* **2018**, *18*, 2990−2998.
(21) Wang, K.; Taniguchi, T.; Watanabe, K.; Kim, P. Engineering Quantum Confinement in Semiconducting Van Der Waals Heterostructure. *arXiv* **2016**, DOI: 10.48550/arXiv.1610.02929.
(22) Zhang, N.; Surrente, A.; Baranowski, M.; Maude, D. K.; Gant, P.; Castellanos-Gomez, A.; Plochocka, P. Moiré Intralayer Excitons in a $MoSe_2$/MoS_2 Heterostructure. *Nano Lett.* **2018**, *18*, 7651−7657.
(23) Jia, G.; Liu, Y.; Gong, J.; Lei, D.; Wang, D.; Huang, Z. Excitonic Quantum Confinement Modified Optical Conductivity of Monolayer and Few-Layered MoS_2. *J. Mater. Chem. C* **2016**, *4*, 8822−8828.
(24) Gopalakrishnan, D.; Damien, D.; Li, B.; Gullappalli, H.; Pillai, V. K.; Ajayan, P. M.; Shaijumon, M. M. Electrochemical Synthesis of Luminescent MoS_2 Quantum Dots. *Chem. Commun.* **2015**, *51*, 6293−6296.
(25) Pallikkarathodi Mani, N.; Ganiga, M.; Cyriac, J. Synthesis of MoS_2 Quantum Dots Uniformly Dispersed on Low Dimensional MoS_2 Nanosheets and Unravelling Its Multiple Emissive States. *ChemistrySelect* **2017**, *2*, 5942−5949.
(26) Sahatiya, P.; Jones, S. S.; Badhulika, S. Direct, Large Area Growth of Few-Layered MoS_2 Nanostructures on Various Flexible Substrates: Growth Kinetics and Its Effect on Photodetection Studies. *Flexible Printed Electron.* **2018**, *3*, No. 015002.
(27) Nguyen, T. P.; Sohn, W.; Oh, J. H.; Jang, H. W.; Kim, S. Y. Size-Dependent Properties of Two-Dimensional MoS_2 and WS_2. *J. Phys. Chem. C* **2016**, *120*, 10078−10085.
(28) Gan, Z. X.; Liu, L. Z.; Wu, H. Y.; Hao, Y. L.; Shan, Y.; Wu, X. L.; Chu, P. K. Quantum Confinement Effects Across Two-Dimensional Planes in MoS_2 Quantum Dots. *Appl. Phys. Lett.* **2015**, *106*, 233113.
(29) Mukherjee, S.; Maiti, R.; Katiyar, A. K.; Das, S.; Ray, S. K. Novel Colloidal MoS_2 Quantum Dot Heterojunctions on Silicon Platforms for Multifunctional Optoelectronic Devices. *Sci. Rep.* **2016**, *6*, 29016.
(30) Kang, J.; Seo, J.-W. T.; Alducin, D.; Ponce, A.; Yacaman, M. J.; Hersam, M. C. Thickness Sorting of Two-Dimensional Transition Metal Dichalcogenides Via Copolymer-Assisted Density Gradient Ultracentrifugation. *Nat. Commun.* **2014**, *5*, 5478.
(31) Fox, D. S.; Zhou, Y.; Maguire, P.; O'Neill, A.; O'Coileain, C.; Gatensby, R.; Glushenkov, A. M.; Tao, T.; Duesberg, G. S.; Shvets, I. V.; Abid, M.; Abid, M.; Wu, H. C.; Chen, Y.; Coleman, J. N.; Donegan, J. F.; Zhang, H. Nanopatterning and Electrical Tuning of

MoS_2 Layers with a Subnanometer Helium Ion Beam. *Nano Lett.* **2015**, *15*, 5307−5313.
(32) Stanford, M. G.; Pudasaini, P. R.; Cross, N.; Mahady, K.; Hoffman, A. N.; Mandrus, D. G.; Duscher, G.; Chisholm, M. F.; Rack, P. D. Tungsten Diselenide Patterning and Nanoribbon Formation by Gas-Assisted Focused-Helium-Ion-Beam-Induced Etching. *Small Methods* **2017**, *1*, No. 1600060.
(33) Zuo, P.; Jiang, L.; Li, X.; Tian, M.; Xu, C.; Yuan, Y.; Ran, P.; Li, B.; Lu, Y. Maskless Micro/Nanopatterning and Bipolar Electrical Rectification of MoS_2 Flakes Through Femtosecond Laser Direct Writing. *ACS Appl. Mater. Interfaces* **2019**, *11*, 39334−39341.
(34) Sunitha, A. P.; Hajara, P.; Shaji, M.; Jayaraj, M. K.; Saji, K. J. Luminescent MoS_2 Quantum Dots with Reverse Saturable Absorption Prepared by Pulsed Laser Ablation. *J. Lumin.* **2018**, *203*, 313−321.
(35) Wei, G.; Czaplewski, D. A.; Lenferink, E. J.; Stanev, T. K.; Jung, I. W.; Stern, N. P. Size-Tunable Lateral Confinement in Monolayer Semiconductors. *Sci. Rep.* **2017**, *7*, 3324.
(36) Song, X. X.; Liu, D.; Mosallanejad, V.; You, J.; Han, T. Y.; Chen, D. T.; Li, H. O.; Cao, G.; Xiao, M.; Guo, G. C.; Guo, G. P. A Gate Defined Quantum Dot on the Two-Dimensional Transition Metal Dichalcogenide Semiconductor WSe_2. *Nanoscale* **2015**, *7*, 16867−16873.
(37) Manouras, T.; Argitis, P. High Sensitivity Resists for EUV Lithography: A Review of Material Design Strategies and Performance Results. *Nanomaterials* **2020**, *10*, 1593.
(38) Lin, Q.; Grigorescu, A. E.; van der Krogt, M. C.; Hagen, C. W. Sub-10-Nm Structures Written in Ultra-Thin HSQ Resist Layers Using Electron-Beam Lithography. In *Advances in Resist Materials and Processing Technology XXIV*; SPIE Advanced Lithography: San Jose, California, United States, 2007; p 65194A.
(39) Zan, R.; Ramasse, Q. M.; Jalil, R.; Georgiou, T.; Bangert, U.; Novoselov, K. S. Control of Radiation Damage in MoS_2 by Graphene Encapsulation. *ACS Nano* **2013**, *7*, 10167−10174.
(40) Komsa, H. P.; Kotakoski, J.; Kurasch, S.; Lehtinen, O.; Kaiser, U.; Krasheninnikov, A. V. Two-Dimensional Transition Metal Dichalcogenides Under Electron Irradiation: Defect Production and Doping. *Phys. Rev. Lett.* **2012**, *109*, No. 035503.
(41) Algara-Siller, G.; Kurasch, S.; Sedighi, M.; Lehtinen, O.; Kaiser, U. The Pristine Atomic Structure of MoS_2 Monolayer Protected from Electron Radiation Damage by Graphene. *Appl. Phys. Lett.* **2013**, *103*, 203107.
(42) Lehnert, T.; Lehtinen, O.; Algara-Siller, G.; Kaiser, U. Electron Radiation Damage Mechanisms in 2D $MoSe_2$. *Appl. Phys. Lett.* **2017**, *110*, No. 033106.
(43) Shcherbakov, D.; Stepanov, P.; Weber, D.; Wang, Y.; Hu, J.; Zhu, Y.; Watanabe, K.; Taniguchi, T.; Mao, Z.; Windl, W.; Goldberger, J.; Bockrath, M.; Lau, C. N. Raman Spectroscopy, Photocatalytic Degradation, and Stabilization of Atomically Thin Chromium Tri-Iodide. *Nano Lett.* **2018**, *18*, 4214−4219.
(44) Man, M. K. L.; Deckoff-Jones, S.; Winchester, A.; Shi, G.; Gupta, G.; Mohite, A. D.; Kar, S.; Kioupakis, E.; Talapatra, S.; Dani, K. M. Protecting the Properties of Monolayer MoS_2 on Silicon Based Substrates with an Atomically Thin Buffer. *Sci. Rep.* **2016**, *6*, 20890.
(45) Castellanos-Gomez, A.; Buscema, M.; Molenaar, R.; Singh, V.; Janssen, L.; van der Zant, H. S. J.; Steele, G. A. Deterministic Transfer of Two-Dimensional Materials by All-Dry Viscoelastic Stamping. *2D Mater.* **2014**, *1*, No. 011002.
(46) Selig, M.; Berghäuser, G.; Raja, A.; Nagler, P.; Schüller, C.; Heinz, T. F.; Korn, T.; Chernikov, A.; Malic, E.; Knorr, A. Excitonic Linewidth and Coherence Lifetime in Monolayer Transition Metal Dichalcogenides. *Nat. Commun.* **2016**, *7*, 13279.
(47) Tinoco, M.; Maduro, L.; Masaki, M.; Okunishi, E.; Conesa-Boj, S. Strain-Dependent Edge Structures in MoS_2 Layers. *Nano Lett.* **2017**, *17*, 7021−7026.
(48) Zhang, C.; Johnson, A.; Hsu, C.-L.; Li, L.-J.; Shih, C.-K. Direct Imaging of Band Profile in Single Layer MoS_2 on Graphite: Quasiparticle Energy Gap, Metallic Edge States, and Edge Band Bending. *Nano Lett.* **2014**, *14*, 2443−2447.
(49) Wu, D.; Li, X.; Luan, L.; Wu, X.; Li, W.; Yogeesh, M. N.; Ghosh, R.; Chu, Z.; Akinwande, D.; Niu, Q.; Lai, K. Uncovering Edge States and Electrical Inhomogeneity in MoS_2 Field-Effect Transistors. *Proc. Nat. Acad. Sci. U. S. A.* **2016**, *113*, 8583.
(50) Mahatha, S. K.; Menon, K. S. R. Inhomogeneous Band Bending on MoS_2(0001) Arising from Surface Steps and Dislocations. *J. Phys.: Condens. Matter* **2012**, *24*, No. 305502.
(51) Grüning, M.; Attaccalite, C. Second Harmonic Generation in hBN and MoS_2 Monolayers: Role of Electron-Hole Interaction. *Phys. Rev. B* **2014**, *89*, No. 081102.
(52) Moody, G.; Kavir Dass, C.; Hao, K.; Chen, C.-H.; Li, L.-J.; Singh, A.; Tran, K.; Clark, G.; Xu, X.; Berghäuser, G.; Malic, E.; Knorr, A.; Li, X. Intrinsic Homogeneous Linewidth and Broadening Mechanisms of Excitons in Monolayer Transition Metal Dichalcogenides. *Nat. Commun.* **2015**, *6*, 8315.
(53) Smithe, K. K. H.; Krayev, A. V.; Bailey, C. S.; Lee, H. R.; Yalon, E.; Aslan, Ö. B.; Muñoz Rojo, M.; Krylyuk, S.; Taheri, P.; Davydov, A. V.; Heinz, T. F.; Pop, E. Nanoscale Heterogeneities in Monolayer $MoSe_2$ Revealed by Correlated Scanning Probe Microscopy and Tip-Enhanced Raman Spectroscopy. *ACS Appl. Nano Mater.* **2018**, *1*, 572−579.
(54) He, X.; Li, H.; Zhu, Z.; Dai, Z.; Yang, Y.; Yang, P.; Zhang, Q.; Li, P.; Schwingenschlogl, U.; Zhang, X. Strain Engineering in Monolayer WS_2, MoS_2, and the WS_2/MoS_2 Heterostructure. *Appl. Phys. Lett.* **2016**, *109*, 173105.
(55) Vincent, T.; Panchal, V.; Booth, T.; Power, S. R.; Jauho, A.-P.; Antonov, V.; Kazakova, O. Probing the Nanoscale Origin of Strain and Doping in Graphene-hBN Heterostructures. *2D Materials* **2018**, *6*, No. 015022.
(56) Murthy, A. A.; Stanev, T. K.; dos Reis, R.; Hao, S.; Wolverton, C.; Stern, N. P.; Dravid, V. P. Direct Visualization of Electric-Field-Induced Structural Dynamics in Monolayer Transition Metal Dichalcogenides. *ACS Nano* **2020**, *14*, 1569−1576.
(57) Epping, A.; Banszerus, L.; Güttinger, J.; Krückeberg, L.; Watanabe, K.; Taniguchi, T.; Hassler, F.; Beschoten, B.; Stampfer, C. Quantum Transport Through MoS_2 Constrictions Defined by Photodoping. *J. Phys.: Condens. Matter* **2018**, *30*, 205001.
(58) Pisoni, R.; Lee, Y.; Overweg, H.; Eich, M.; Simonet, P.; Watanabe, K.; Taniguchi, T.; Gorbachev, R.; Ihn, T.; Ensslin, K. Gate-Defined One-Dimensional Channel and Broken Symmetry States in MoS_2 Van Der Waals Heterostructures. *Nano Lett.* **2017**, *17*, 5008−5011.
(59) Cui, X.; Lee, G.-H.; Kim, Y. D.; Arefe, G.; Huang, P. Y.; Lee, C.-H.; Chenet, D. A.; Zhang, X.; Wang, L.; Ye, F.; Pizzocchero, F.; Jessen, B. S.; Watanabe, K.; Taniguchi, T.; Muller, D. A.; Low, T.; Kim, P.; Hone, J. Multi-Terminal Transport Measurements of MoS_2 Using a Van Der Waals Heterostructure Device Platform. *Nat. Nanotechnol.* **2015**, *10*, 534−540.
(60) Garcia, A.; Raya, A. M.; Mariscal, M. M.; Esparza, R.; Herrera, M.; Molina, S. I.; Scavello, G.; Galindo, P. L.; Jose-Yacaman, M.; Ponce, A. Analysis of Electron Beam Damage of Exfoliated MoS_2 Sheets and Quantitative Haadf-Stem Imaging. *Ultramicroscopy* **2014**, *146*, 33−38.
(61) Tombros, N.; Veligura, A.; Junesch, J.; Guimarães, M. H. D.; Vera-Marun, I. J.; Jonkman, H. T.; van Wees, B. J. Quantized Conductance of a Suspended Graphene Nanoconstriction. *Nat. Phys.* **2011**, *7*, 697.
(62) van Wees, B. J.; van Houten, H.; Beenakker, C. W. J.; Williamson, J. G.; Kouwenhoven, L. P.; van der Marel, D.; Foxon, C. T. Quantized Conductance of Point Contacts in a Two-Dimensional Electron Gas. *Phys. Rev. Lett.* **1988**, *60*, 848−850.
(63) van Weperen, I.; Plissard, S. R.; Bakkers, E. P. A. M.; Frolov, S. M.; Kouwenhoven, L. P. Quantized Conductance in an InSb Nanowire. *Nano Lett.* **2013**, *13*, 387−391.
(64) Lin, Y.; Ling, X.; Yu, L.; Huang, S.; Hsu, A. L.; Lee, Y.-H.; Kong, J.; Dresselhaus, M. S.; Palacios, T. Dielectric Screening of Excitons and Trions in Single-Layer MoS_2. *Nano Lett.* **2014**, *14*, 5569−5576.

https://doi.org/10.1021/acsami.2c03652
ACS Appl. Mater. Interfaces 2022, 14, 23775−23784

(65) Sui, Y.; Appenzeller, J. Screening and Interlayer Coupling in Multilayer Graphene Field-Effect Transistors. *Nano Lett.* **2009**, *9*, 2973−2977.
(66) Novoselov, K. S.; Geim, A. K.; Morozov, S. V.; Jiang, D.; Zhang, Y.; Dubonos, S. V.; Grigorieva, I. V.; Firsov, A. A. Electric Field Effect in Atomically Thin Carbon Films. *Science* **2004**, *306*, 666.
(67) Li, X.; Zhu, H. Two-Dimensional MoS_2: Properties, Preparation, and Applications. *J. Materiomics* **2015**, *1*, 33−44.

https://doi.org/10.1021/acsami.2c03652
ACS Appl. Mater. Interfaces 2022, 14, 23775−23784